

Crack Growth Rates in a PWR Environment of Nickel Alloys from the Davis-Besse and V.C. Summer Power Plants

Argonne National Laboratory

**U.S. Nuclear Regulatory Commission
Office of Nuclear Regulatory Research
Washington, DC 20555-0001**



Crack Growth Rates in a PWR Environment of Nickel Alloys from the Davis-Besse and V.C. Summer Power Plants

Manuscript Completed: November 2005
Date Published: November 2006

Prepared by
B. Alexandreanu, O. K. Chopra and W. J. Shack

Argonne National Laboratory
9700 South Cass Avenue
Argonne, IL 60439

W.H. Cullen, Jr., NRC Project Manager

Prepared for
Division of Fuel, Engineering and Radiological Research
Office of Nuclear Regulatory Research
U.S. Nuclear Regulatory Commission
Washington, DC 20555-0001
NRC Job Code Y6388



Crack Growth Rates of Nickel Alloys in a PWR Environment from the Davis-Besse and V.C. Summer Power Plants

by

B. Alexandreanu, O. K. Chopra, and W. J. Shack

Abstract

In light water reactors (LWRs), vessel internal components made of nickel-base alloys are susceptible to environmentally assisted cracking. A better understanding of the causes and more effective mechanisms of this cracking may permit more accurate assessments of damage accumulation and requirements on inspection intervals. A program is under way at Argonne National Laboratory to evaluate the resistance of Ni alloys and their welds to environmentally assisted cracking in simulated LWR coolant environments. This report presents crack growth rate (CGR) results for the following nickel alloys tested in a simulated LWR environment: Alloy 600 removed from the Davis-Besse control rod drive mechanism nozzle #3, Alloy 182 from a J-groove weld nozzle #11 from Davis-Besse, and Alloys 182 and 82 from a hot-leg nozzle-to-pipe weld of the V.C. Summer reactor coolant system. The results from the present study are compared with the existing CGR data for Ni alloys to determine the relative susceptibility of these particular heats of material to environmentally enhanced cracking. Under cyclic loading, the Alloy 600 nozzle exhibited significant environmental enhancement, but little or no environmental enhancement was evident for the weld alloys from both Davis-Besse and V.C. Summer. Under constant load, the CGRs of the Alloy 600 nozzle are a factor of 4–8 higher than the median CGRs based on all the available data for Alloy 600 materials. This material exhibited predominantly intergranular fracture, even during precracking under cyclic loads. For both the Davis-Besse and V.C. Summer weld alloys, the CGRs under constant load are lower than those predicted by the disposition curve proposed for Alloy 182 weld metals.

This page is intentionally left blank.

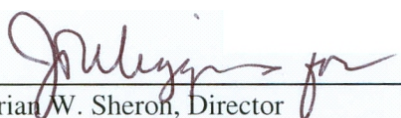
Foreword

This report presents crack growth rate (CGR) data and the corresponding fracture surface and metallographic examinations from cyclic loading and primary water stress-corrosion cracking (PWSCC) tests of specimens taken from structural components of (1) the vessel head from the Davis-Besse plant, which was discarded in 2002, and (2) pieces of the hot leg “A” weld joint at the V.C. Summer plant, which was found cracked and leaking in 2001. In both cases, specimens were removed adjacent to the degraded regions of these components, and tested in simulated pressurized-water reactor coolant at a temperature similar to that at which the component operated in the plant. Specifically, the specimens from the Davis-Besse reactor were tested at 316°C (600°F) and the specimens taken from the V.C. Summer weld were tested at 320°C (608°F).

At the Davis-Besse plant, Alloy 600 (A600) vessel head penetration nozzles #1, #2, #3 and #4, located at or near the top center of the reactor pressure vessel head, exhibited a number of cracks of varying sizes. Specimens were cut from nozzle #3 and tested as part of this test program. Other test specimens were cut from the Alloy 182 (A182) J-groove penetration weld from nozzle #11, located immediately downhill from nozzle #3, which also exhibited visible cracks at the wetted surface. Metallography and tensile test results on these materials indicate that the yield and ultimate strength, elongation, and microstructural properties, including phase identification and chemistry, are within specification. However, the PWSCC crack growth rates for the A600 from nozzle #3 are generally very high — at the 95th percentile of the log-normal distribution of coefficients expressing crack growth rates in this type of alloy. However, the crack growth rate data exhibit considerable scatter, including some segments of the test producing no measurable growth, even though the test conditions favored readily observable crack extension.

The crack growth rates for the A182 weld metal specimens from the Davis-Besse penetration weld, and the A182 and Alloy 82 (A82) portions of the V.C. Summer hot leg weld, were generally less than the median growth rate of the log-normal distribution of coefficients expressing crack growth rates in A182 and A82 weld metals. The CGR results obtained by Argonne National Laboratory are also less than results on the same materials measured at Westinghouse’s Science and Technology Center in 2004. No specific reason for this difference could be identified, other than acknowledging the substantial experimental scatter witnessed in CGR tests at all laboratories engaged in this type of research.

The impetus for this research on PWSCC comes from the need to evaluate reactor-aged. This topic may be an especially important consideration in the review of license applications, as well as the disposition of relief requests pertaining to flaw evaluations for vessel penetration and piping butt welds. The data on cyclic loading effects are commonly used in the fatigue analyses required for flaw evaluations that are completed in accordance with the requirements set forth in Section XI, IWB-3660 and Appendix O, of the Boiler and Pressure Vessel Code promulgated by the American Society of Mechanical Engineers.



Brian W. Sherrin, Director
Office of Nuclear Regulatory Research
U.S. Nuclear Regulatory Commission

This page is intentionally left blank.

Contents

Abstract	iii
Foreword	v
Executive Summary	xv
Acknowledgments	xvii
Abbreviations	xix
1. Introduction.....	1
2. Experimental.....	5
2.1 Materials.....	5
2.1.1 Davis-Besse CRDM Nozzle and J-Groove Weld.....	5
2.1.2 V.C. Summer Reactor Vessel Nozzle-to-Pipe Weld	6
2.2 Specimen Geometry	8
2.2.1 Davis-Besse Alloys	8
2.2.2 V.C. Summer Alloys.....	12
2.3 Test Facilities.....	13
2.3.1 CGR Test Facility with a 1-Liter Autoclave.....	13
2.3.2 CGR Test Facility with a 6-Liter Autoclave.....	15
2.4 Test Procedure	17
3. Microstructural Characterization.....	21
3.1 Davis-Besse CRDM Nozzle and J-Groove Weld Alloys.....	21
3.2 V.C. Summer Reactor Vessel Nozzle-to-Pipe Weld Alloys.....	28
4. Results.....	33
4.1 Tensile Data	33
4.1.1 Alloy 600 from CRDM Nozzle #3 and Alloy 182 from the Nozzle #11 J-Groove Weld.....	33
4.1.2 Alloys 82 and 182 from the V.C. Summer Nozzle-to-Pipe Weld and Butter	35
4.2 Crack Growth Data.....	36

4.2.1	Davis–Besse CRDM Nozzle Alloy 600	36
4.2.2	Davis–Besse J–Groove Weld	45
4.2.3	V.C. Summer Nozzle–to–Pipe Weld	55
5	Discussion.....	67
5.1	Alloy 600 from the Davis-Besse CRDM Nozzle #3	67
5.2.	Fatigue Crack Growth Rates for Ni–alloy Weld Metals in Air	68
5.3	Ni–Alloy Welds	70
5.3.1	From the Davis–Besse CRDM Nozzle #11	70
5.3.2	From the V.C. Summer Reactor Vessel Nozzle–to–Pipe Weld.....	71
5.4	Variability in Ni-Alloy CGR Data.....	73
6	Summary	75
	References	77

Figures

1..	Photographs of the ring from Davis–Besse CRDM Nozzle #3.....	5
2.	Photographs of the ring from Davis–Besse CRDM Nozzle #3 and reactor pressure vessel head sample with J–groove weld from Nozzle #11.	5
3.	Photographs of the V.C. Summer spool piece.....	7
4.	Schematic diagram of the V.C. Summer hot–leg nozzle–to–pipe weld in the reactor coolant system.	7
5.	Configurations of the 1/2–T and 1/4–T compact tension specimen.	8
6.	Configurations of the tensile specimen with a 20.3-mm and a 12.7-mm gauge length.....	9
7.	Orientation and location of the mechanical–test specimens obtained from Davis–Besse CRDM Nozzle #3 and the J–groove weld of Nozzle #11.....	10
8.	Orientation and location of the mechanical–test specimens from the J–groove weld of nozzle #11 on which defects were found during fabrication.....	10
9.	Approximate locations where defects were found during fabrication of test specimens from CRDM Nozzle #11 J–groove weld.	10
10.	Large defect found on the fracture surface of tensile Specimen J11TL-4, the cause of a significant loss of ductility.....	11
11.	Structural defects on the face and side surface of the specimen blanks used for machining CT specimens.	11
12.	Schematic of the tensile specimens fabricated from the V.C. Summer weld piece for “C” and “L” orientations.	12
13.	Schematic of the CT specimens fabricated from the V.C. Summer weld piece for “L” and “C” orientations.	12
14.	Photograph of the specimen load train for the 1–liter autoclave.....	13
15.	Schematic diagram of the recirculating water system.	14
16.	Photograph of the specimen load train.....	16
17.	Schematic diagram of the recirculating autoclave system used for CGR tests.	16
18.	Orientation of the planes on which metallography was conducted on material originating from Davis–Besse CRDM Nozzle #3 and the J–groove weld of Nozzle #11.....	21
19.	Microstructures observed on planes 03-1 and 03-2 of the CRDM nozzle alloy.	22
20.	Ti-rich precipitates observed in the matrix and grain boundary of the nozzle alloy.....	22
21.	X-ray spectra obtained from Alloy 600 bulk and a Ti-rich matrix precipitate.....	23

22.	Microstructures observed on planes 03-3 and 03-4 of the J-groove weld alloy.....	24
23.	Higher magnification microstructures observed on planes 03-3 and 03-4 of the J-groove weld alloy.....	25
24.	Microstructures observed on plane 03-4 for the J-groove weld of Nozzle #11.....	26
25.	Micrograph showing the locations where x-ray spectra were collected and spectra from background, matrix precipitate, grain boundary precipitate, another matrix precipitate, and background at the completion of this series of analyses.....	27
26.	Schematic showing the locations of the metallography samples cut from the V.C. Summer weld piece.	28
27.	Microstructure of the butter alloy in Sample #1.....	28
28.	Microstructure of the butter alloy in Sample #3.....	29
29.	Microstructure of the weld alloy in Sample #2.	30
30.	Microstructure of the weld alloy in Sample #5.	30
31.	Microstructure of the interface between the butter and weld alloys in Sample #4.	31
32.	Examples of defects in the weld alloy in Sample #2.	32
33.	Grain boundary sliding at the weld-pipe interface.	32
34.	Engineering stress vs. strain curve at 316°C for Alloy 600 from Davis-Besse CRDM Nozzle #3 in the “L” orientation.	33
35.	Engineering stress vs. strain curves at 316°C for Alloy 182 from the Davis-Besse CRDM Nozzle #11 J-groove weld in “L” and “C” orientations.....	34
36.	Fracture surfaces of Alloy 182 Specimens J11TL-4, J11TC-1, and J11TC-2 from the Davis-Besse CRDM Nozzle #11 J-groove weld.	34
37.	Engineering stress vs. strain curves at 316°C for Alloy 182 and 82 specimens from the butter and weld regions of the V.C. Summer nozzle-to-pipe dissimilar metal weld.....	35
38.	Crack length vs. time for Specimen N3CL-1 in simulated PWR environment at 320°C during test periods precracking-2, 3-4, 5, and 6-7.	36
39.	Micrograph of the fracture surface of Specimen N3CL-1.	38
40.	Examples of transition from a TG to an IG fracture mode in Specimen N3CL-1.	38
41.	Crack length vs. time for Specimen N3CC-2 in a simulated PWR environment at 320°C during test periods 1-4, 5-8, and 10-11.	39
42.	Micrograph of the fracture surface of Specimen N3CC-2.....	41
43.	Fracture surface of Specimen N3CC-2 and high-magnification micrographs at locations A and B.	41

44.	Crack length vs. time plots for Specimen N3CC-3 of Alloy 182 in PWR water at 316°C during test periods precracking-1, 2-5, and 6-7.....	42
45.	Micrograph of the fracture surface of Specimen N3CC-3.....	43
46.	Micrograph showing a portion of the fracture surface of Specimen N3CC-3 and high-magnification micrographs at locations 1, 2, and 3.	44
47.	Crack length vs. time plots for Specimen J11CC-1 of Alloy 182 J-groove weld in PWR water at 316°C during test periods precracking, 1-3a, 3b-7, 8-11, and 12-13.....	46
48.	Crack front on Sample J11CC-1.	47
49.	Crack morphology at position A: mixed IG and TG; mixed IG and TG, secondary cracks; and high-magnification micrograph showing the boxed area in (b).....	48
50.	Crack morphology at position B: mixed IG and TG, and high-magnification micrographs at locations indicated by arrows in (a).	49
51.	Crack morphology at position C: mixed IG and TG, mixed IG and TG, and striations on the fracture surface.	50
52.	Crack length vs. time plots for Specimen J11CC-3 of Alloy 182 in PWR water at 316°C during precracking and test periods 1, 2-4, 5-7, and 8-13.	52
53.	Micrograph of the cross section of Specimen J11CC-3 showing the fracture-plane profile	53
54.	Micrograph of the fracture surface of Specimen J11CC-3 tested in PWR water at 316°C.....	53
55.	Micrographs showing a slice of the entire length of the fracture surface and high-magnification micrographs of the surface at select locations.....	54
56.	Micrographs showing IG secondary cracks parallel to the crack front in Specimen J11CC-3 tested in PWR water at 316°C.....	55
57.	Crack length vs. time for Alloy 82 nozzle-to-pipe weld specimen in simulated PWR environment at 320°C during test periods precrack-2 and 3-4.	56
58.	Micrograph of the fracture surface of Specimen WCR-01.....	57
59.	Micrographs of portion of the fracture surface of Specimen WCR-01 and higher magnification of position 1 and position 2.	57
60.	Crack length vs. time for Alloy 182 butter specimen in simulated PWR environment at 320°C during precracking and test periods 1, 2-4, 5-7, 8-10, and 11-12.....	59
61.	Cross section of the V.C. Summer Alloy 182 butter Specimen BCR-01.	61
62.	Micrograph of the fracture surface of Specimen BCR-01.....	61
63.	Micrographs of the fracture surface of Specimen BCR-01 at locations 1 and 2 in Fig. 62.....	62

64.	Crack length vs. time for Alloy 82 weld Specimen WLR-01 in simulated PWR environment at 320°C during precracking, precracking and 1–3, 4, 5, 6–7, 8-9, 11–13, and 14.....	63
65.	Micrograph of the fracture surface of the weld V.C. Summer Specimen WLR–01.....	66
66	Micrographs of the fracture surface of Specimen BCR–01 at locations 1 and 2 in Fig. 65.....	66
67.	CGR data for Davis–Besse CRDM Nozzle #3 Alloy 600 in PWR water at 316°C under cyclic loading.....	67
68.	CGR data for Davis–Besse CRDM Nozzle #3 Alloy 600 in PWR water at 316°C under constant load and log–normal distribution of constant α for 26 heats of Alloy 600.	68
69.	Variation of normalized constant C for Ni–alloy weld metals with temperature.	69
70.	Predicted–vs.–experimental values of fatigue CGR of Ni–alloy weld metals in air and PWR environment under predominantly mechanical fatigue loading conditions.....	69
71.	Experimental–vs.–predicted values of fatigue CGR of Alloy 182 and Alloy 82 in air and PWR environment.	70
72.	Cyclic CGR data for Alloy 182 from the Davis–Besse CRDM Nozzle #11 J–groove weld in a PWR environment at 316°C under cyclic loading and constant load.....	71
73.	Fatigue CGR data for V.C. Summer Ni–alloy welds in a PWR environment plotted as a function of the growth rate for Ni-alloy welds in air under the same loading conditions.....	72
74.	CGR data for Alloy 182 and 82 nozzle-to-pipe butter and weld specimens from V.C. Summer in a PWR environment at 325°C under constant load, and log–normal distribution of constant α for several heats of Alloys 82 and 182.	72
75.	Micrographs from the fracture surface of weld specimens: Davis–Besse Specimen J11CC-1 and V.C. Summer Specimen BCR–01.....	74

Tables

1.	Chemical composition and tensile properties of Alloy 600 from Davis–Besse CRDM Nozzle #3.	6
2.	Chemical composition and tensile properties of Alloy 182 from the Davis–Besse CRDM Nozzle #11 J–groove weld.	6
3.	Chemical composition and tensile properties of Alloy 82 weld metal from the V.C. Summer hot–leg nozzle–to–pipe weld.	7
4.	Chemical composition and tensile properties of Alloy 182 butter from the V.C. Summer hot–leg nozzle–to–pipe weld.	8
5.	Radiological survey report for the V.C. Summer spool piece.	13
6.	Chemical composition of the bulk material and matrix precipitates obtained from EDX analyses of the Nozzle #3 Alloy 600.	23
7.	Chemical compositions of the bulk material and matrix and grain boundary precipitates.	27
8.	Tensile test results at 316°C for Alloys 600 and 182 removed from the Davis-Besse CRDM nozzle and J–groove weld.	33
9.	Tensile test results at 316°C for Alloys 182 and 82 removed from the V.C. Summer nozzle–to–pipe dissimilar metal weld.	35
10.	CGR data for 1/4–T CT specimen N3CL-1 of Alloy 600 in PWR water at 316°C.	36
11.	CGR data for 1/4–T CT Specimen N3CC-2 of Alloy 600 in PWR water at 316°C.	39
12.	CGR data for Specimen N3CC-3 in PWR water at 316°C.	42
13.	CGR data for Specimen J11CC-1 of Alloy 182 J–groove weld in PWR water at 316°C.	45
14.	CGR data for Specimen J11CC-3 in PWR water at 316°C.	51
15.	CGR data for Specimen WCR–01 of the Alloy 82 SMA weld in PWR water at 320°C.	55
16.	CGR data for Specimen BCR–01 of the Alloy 182 SMA weld in PWR water at 320°C.	58
17.	CGR data for Specimen WLR–01 of the Alloy 82 SMA weld in PWR water at 320°C.	62

This page is intentionally left blank.

Executive Summary

The Ni–base alloys used as construction materials in light water reactors (LWRs) have experienced stress corrosion cracking (SCC). Such cracking was first observed in steam generator tubes, but it has also occurred in Ni alloys used in applications such as instrument nozzles and heater thermal sleeves in the pressurizer and for control–rod drive mechanisms (CRDMs) and other penetrations in the reactor vessel closure heads. In operating plants, the weld metal Alloys 82 and 182 are used with Alloy 600. On the basis of current operating experience, these materials appear to be more resistant to environmentally assisted cracking than the wrought alloy. However, laboratory tests indicate that in pressurized water reactor (PWR) coolant environments, the SCC susceptibility of Alloy 182 may be greater than Alloy 600, and Alloy 82 may be comparable to Alloy 600. This apparent inconsistency between field and laboratory experience is an issue that needs further investigation.

A program is under way at Argonne National Laboratory (ANL) to evaluate the resistance of Ni alloys and their welds to environmentally assisted cracking in simulated LWR coolant environments. This report presents crack growth rate (CGR) results for Alloy 600 and Alloy 182 weld metal alloys in simulated PWR environments at 316 or 320°C. The tests were performed with Alloy 600 from Davis–Besse CRDM Nozzle #3, Alloy 182 from a J–groove weld in Davis–Besse Nozzle #11, and Alloys 182 and 82 from a hot–leg nozzle–to–pipe weld in the V.C. Summer reactor coolant system. The total crack extensions estimated by the direct current (DC) potential method were verified by physical measurements on the fracture surfaces.

The objective of this study was to determine whether the crack growth in these materials from the Davis–Besse and V.C. Summer plants are consistent with our understanding of CGRs in Ni–alloy and welds. The results are compared with the existing SCC CGR data to determine the relative susceptibility of these alloys to primary water stress corrosion cracking (PWSCC). The cyclic CGR behavior was also examined. The existing cyclic crack growth data for Ni–alloy welds in air were analyzed to develop correlations to determine the fatigue CGRs as a function of loading conditions and temperature. In air, the growth rates of weld alloys are a factor of ≈ 2.5 greater than those of Alloy 600 under similar loading conditions. The results of a detailed metallographic examination of the alloys to characterize their microstructure and fracture morphology are also presented.

The Davis–Besse nozzle alloy showed significant environmental enhancement of fatigue CGRs, and the SCC growth rates (i.e., CGRs under constant load) were a factor of 4–8 higher than those of the median curve for Alloy 600. These rates correspond to the ≈ 95 th percentile values of the population; i.e., the nozzle material exhibits very high susceptibility to SCC compared to other heats of Alloy 600. A unique feature of the nozzle alloy is that it exhibits a predominantly intergranular fracture even during fatigue loading. Transgranular growth is observed at the very beginning of the test (i.e., near the machine notch), but, in most cases, the crack becomes intergranular when the first grain boundary is encountered. The fact that intergranular growth takes place in a regime dominated by mechanical fatigue (which normally results in transgranular growth) suggests that the grain boundaries must have suffered some form of sensitization either during fabrication and/or during two decades in service. The reason for the high growth rates for the nozzle alloy is not clear. Metallographic examination of the Davis–Besse CRDM nozzle #3 Alloy 600 revealed a “good” microstructure, i.e., extensive grain–boundary coverage of Cr–rich carbides, and relatively low or average tensile strength. These conditions are typically associated with low susceptibility of the material to PWSCC. Differences in the microstructure in terms of extent and nature of carbide precipitation may be important.

The weld alloys from the Davis–Besse and V.C. Summer plants show typical dendritic microstructure. Under predominantly mechanical fatigue loading conditions (low load ratios and high frequency), the CGRs for the Davis–Besse J–groove weld alloy are comparable and those for the V.C. Summer weld alloys are a factor of ≈ 5 lower than the growth rates typically observed for laboratory–prepared Alloy 182 or 82 welds. The cyclic CGRs for Alloy 182 and Alloy 82 weld specimens from both the Davis–Besse CRDM nozzle J–groove weld and the V.C. Summer reactor vessel nozzle–to–pipe weld showed very little environmental enhancement.

The SCC CGRs for most of the welds investigated were found to be approximately an order of magnitude lower than the proposed CGR disposition curve for these weld materials. The growth rates correspond to the ≈ 10 th to 25th percentile of the various heats used in developing the disposition curve; i.e., the field weld alloys exhibit low susceptibility to SCC. For the specimens with low CGRs, cracks were observed on the fracture surface, parallel to the crack front and transverse to the crack plane. At present, it is not clear whether these are preexisting cracks (e.g., hot cracks) or whether they were formed during the tests (e.g., by crack branching at the crack tip). In any case, these out–of–plane cracks appear to impede crack advance and may be responsible for the low CGRs in the material. Such cracks are not observed on the fracture surface of the specimen with growth rates above the median value.

Acknowledgments

The authors thank E. J. Listwan, T. M. Galvin, J. Tezak, E. E. Gruber, A. Hins, and R. Clark for their contributions to the experimental effort. This work is sponsored by the Office of Nuclear Regulatory Research, U.S. Nuclear Regulatory Commission, under Job Code Y6388; Program Manager: W. H. Cullen, Jr.

This page is intentionally left blank.

Abbreviations

ANL	Argonne National Laboratory
ASME	American Society of Mechanical Engineers
ASTM	American Society for Testing and Materials
BWR	Boiling Water Reactor
C	Circumferential
CGR	Crack Growth Rate
CRDM	Control Rod Drive Mechanism
CT	Compact Tension
DO	Dissolved Oxygen
ECP	Electrochemical Potential
EDX	Energy Dispersive X-Ray
GBC	Grain Boundary Coverage
GBCD	Grain Boundary Character Distribution
ID	Inner Diameter
IG	Intergranular
L	Longitudinal
LWR	Light Water Reactor
MRP	Materials Reliability Performance
NRC	U.S. Nuclear Regulatory Commission
NWC	Normal Water Chemistry
OD	Outer Diameter
PWSCC	Primary Water Stress Corrosion Cracking
PWR	Pressurized Water Reactor
R	Radial
RTZ	Roll Transition Zone
SA	Solution Annealed
SCC	Stress Corrosion Cracking
SEM	Scanning Electron Microscope
SHE	Standard Hydrogen Electrode
SS	Stainless Steel
TG	Transgranular

This page is intentionally left blank.